

Fast solvers for Tokamak fluid models with PETSC – Part I

Mark F. Adams¹, Jin Chen², and Benjamin Sturdevant³

¹Lawrence Berkeley National Laboratory, Berkeley CA

²Princeton Plasma Physics Laboratory, Princeton NJ

³Rensselaer Polytechnic Institute, SCOREC, Troy NY

Abstract

This report develops the first step in adding multigrid solvers to scientific and engineering-relevant magnetohydrodynamics (MHD) models of Tokamaks. These models are characterized by a distinguished direction in the toroidal coordinate that is partially aligned with the magnetic guide field, which dominates the plasma dynamics. All Tokamak models exploit this structure, for example, *NIMROD*¹ uses *2D*, unstructured, high-order finite elements in the poloidal plane with Fourier modes in the toroidal coordinate, and the *3D*, extended MHD code *M3D-C1*² uses *2D*, unstructured C^1 elements in the poloidal plane with cubic Hermite functions in the toroidal direction. This structure suggests adding toroidal semi-coarsening multigrid to the existing solver and thereby reducing reliance on direct solvers, which do not scale optimally and are not well suited to modern hardware that demands extreme levels of parallelism. This report focuses on the velocity solve in *M3D-C1*, using the PETSC – the Portable, Extensible Toolkit for Scientific Computation – numerical library³, and shows that with little new application code, one-dimensional multigrid is about $5x$ faster than the existing one-level method on an MHD disruption, with runaway electrons, test problem.

1 Introduction

The *M3D-C1* MHD fusion energy sciences application models Tokamak plasmas with unstructured meshes of simplicies in the poloidal plane that are extruded in the toroidal direction with aspect ratios on the order of 10^2 and are thus highly anisotropic. These prism elements use a 2D C^1 continuity Bell element in the poloidal plane [5] with cubic Hermite elements in the toroidal direction [7]. These discretizations have not only the variable as a degree of freedom (DoF), the zeroth derivative, but higher derivatives for a total of 12 DoFs per vertex per variable. There are several solves in the *M3D-C1* numerical method, but the velocity, or momentum, solve is the most challenging and the focus of this work.

The first step in developing solvers for *M3D-C1* is to exploit the regular grid in the toroidal direction with the use of geometric, semi-coarsening multigrid [8]. Computing a Jacobian matrix with the application code on coarse grids is not practical and therefore they are constructed with an algebraic, Galerkin process. The second step in developing a multigrid method is the design of a multigrid smoother. Line smoothers,

¹<https://nimrodteam.org/>

²<https://w3.pppl.gov/~nferraro/m3dc1.html>

³<https://petsc.org>

block Jacobi solvers with blocks that follow field lines, are the traditional approach to anisotropies with multigrid, but for simplicity we opt for point block Jacobi (PBJ) smoothers: with small (36 equations) vertex blocks with exact, dense subdomain solves.

The 3D velocity field is decomposed into three stream functions, which represent waves in the model. This model can use one, two or all three stream functions; using all three is common in practice. With these coordinates, on a Cartesian grid without nonlinear terms, the three variables decoupled and in Tokamak geometry with nonlinear terms the variables are weakly coupled §B. Because of this weak coupling, *FieldSplit* preconditioners in PETSC, that treat each variable separately with a (3) block Gauss-Seidel iteration, are viable. With *FieldSplit*, a 12 DoF per vertex PBJ sub-solver is used. A second options is to treat the system monolithically, resulting in one, 36 DoF per vertex PBJ smoother.

The structured toroidal grid make semi-coarsening geometric multigrid (MG) particularly simple, with geometric 2:1 coarsening and a 3-point stencil⁴ prolongation operator P . Note, NIMROD exploits this structure in the formulation, before the algebraic solver, however the resulting 2D linear solve is somewhat similar to a poloidal plane solve in *M3D-C1*, in that the basis functions are nearly orthogonal and coupled with nonlinear terms. Given P , which is the only new numerical code needed in *M3D-C1*, the coarse grids can be constructed recursively with a Galerkin process: $A_{i+1} = P^T A_i P$, resulting in a geometric/algebraic MG solver with a purely algebraic interface [1].

This report proceeds by describing the *M3D-C1* velocity evolution equations and solver methods in §2, the model problem for performance evaluation and verification is defined in §3, CPU performance results are presented in §4, results with GPUs are presented in §5 and §6 concludes the report.

2 *M3D-C1* equations and solver issues

While iterative solvers have the potential to be effective PDE solvers, they require understanding the equations and the discretizations to achieve their potential. Give the equations and discretizations analyses techniques are available to guide the design of and even prove the optimality of multigrid methods, such as local Fourier analysis (p. 98 [8]), h-ellipticity (p. 121 [8]), principle component analysis, which in this context is writing your equations in matrix form and taking the determinant and order the terms to understand the fundamental nature of the system (e.g., is it elliptic). This process is arduous for *M3D-C1*, see §A for a partial documentation of this process, and no particularity application specific techniques are used in this work.

At a high level, the equations to solved are of the form in (16) and (17). When \mathbf{v} is expanded with (19) a 3×3 block system results, which is preconditioned with block system of the form (25) in a *FieldSplit* smoother or a monolithic PBJ smother. These smoothers need only be approximate solves and the coarsest grid must be solved exactly.

The nature of these blocks is of interest in designing optimal solvers, but the complexity of the these is beyond the scope of this work and we rely on standard MG methods. Be that as it may, we can look at the diagonal blocks of our system, δW_{11} in (26), δW_{22} in (27) and δW_{33} in (28), and observe that they have Laplacian, ϕ in (27), and bi-Harmonic like equations with curls in (26) and(28). While Adler et al. have developed multigrid methods for a two field viscoresistive MHD model [4], and Chacon has use

⁴]₂ 1 ₂ [

parabolization to use a multigrid solver for the Laplacian [6], there is no prior work on solving matrices approaching the complexity of these $M3D-C1$ matrices with multigrid.

Field splitting solvers. Solves with multiple equations, that are not a simple vector field, are supported in PETSC's *FieldSplit* preconditioner. Stokes equation for incompressible flow is a standard problem for these solvers and Schur compliments are commonly used, but they are not practical for the complicated equations in M3D-C1 and (big block) Gauss-Seidel (GS) is the only practical option. Fortunately GS converges well for strongly diagonally dominant problems, which these problems are. Analysis shows that the norm of the off-diagonal blocks in (25) are of the order of the ratio of the minor to major radius of the Tokamak ($\sim \frac{1}{6}$ for common Tokamaks) squared and we have verified this on our test problems where we find the norms of off-diagonal blocks to be at most $\sim 1\%$. See Appendix §B for details. While *FieldSplit* has some attractive properties, we have found them to be slightly slower than the simpler point block Jacobi smoothers, which we use in this study.

Point block Jacobi: The final major component of our solver approach is to use PBJ smoothers. With an unstructured mesh of triangle elements all of the degrees of freedom are on the vertices of the triangles. The Bell elements are about fifth order accurate (in plane) and the cubic splines are fourth order accurate. This discretization has 12 DoFs per vertex and with three equations in the velocity solve the matrix has a block size of 36. PBJ smoothers in PETSC compute explicit, dense inverses of small diagonal blocks of the matrix, which can be applied effectively on GPUs, with dense BLAS2 linear algebra.

3 Model test problem

During the sudden loss of confinement in a tokamak, the growth of a relativistic electron population called runaways often occurs with accompanying magnetohydrodynamic activity, as seen on machines such as JET and DIII-D. Runaway electrons (REs) and magnetohydrodynamic instabilities interact in a complicated manner, and how this interaction affects the final runaway current is not well-understood. In this simulation, we perform self-consistent magnetohydrodynamic and runaway electron simulations using $M3D-C1$. In the test problem used for verification and performance studies in §4, runaway electron growth occurs in a saw-teething disruption plasma, and the interactions between these two effects are quantified in physics studies. Figure 1 shows snapshots of the magnetic field topology and RE current. The velocity

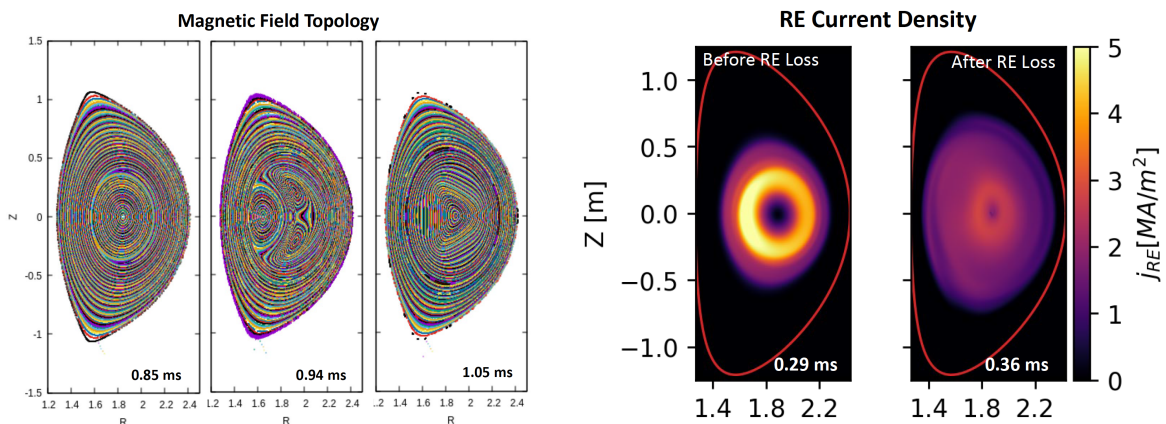


Figure 1: Snapshots of fields during thermal quench and runaway electron generation (courtesy R. Datta)

in the solver studied here produces a current that is modified with a model of RE current in the project that supplied these test cases.

4 Performance evaluation

M3D-C1 evolves the velocity solve according to (18), where a Jacobian matrix is recomputed at every time step, without a non-linear solver iteration (eg, one Newton iteration only). The solver setup for the current production, block Jacobi (BJ), *M3D-C1* solver is dominated by a full plane direct solver factorization on each plane. The MG solver requires a direct solver for the coarse grid, one full plane, and given that subdomains are relatively small, this cost is nearly the same as the BJ factorizations (ie, the need for only one plane solve in MG is of little benefit). The MG solver also has a significant extra cost of the Galerkin coarse grid construction. Again, because the process subdomains are relatively small, MG solve times per iteration on coarse grids and coarse grid construction are about the same as their fine grid counterpart. This results in about $\log(N)$ time scaling, with N planes, rather than the theoretical 1D multigrid complexity: the geometric sum $1 + \frac{1}{2} + \dots \approx 2$.

Solver setup. This solver setup phase is relatively expensive and is lagged with a constant *refresh period*. This results in degradation of the convergence rate before a solver refresh restores a consistent solver. This degradation is more pronounced in the MG solver and in fact the MG solves converge in one iteration in these test, but are constrained to take a minimum of two iterations.

FieldSplit. Performance experiments are restricted to the current production BJ solver and the MG solver with the PBJ smoother. The *FieldSplit* smoother is slightly slower and not investigated here, but *FieldSplit* could be useful in the future with larger PBJ domains because vertex blocks of the matrix are $9x$ smaller than the monolithic smoother.

Solver tolerance and verification. The solver tolerance for each solver (BJ vs MG) is chosen so as to pass an *M3D-C1* verification test where several quantities (kinetic and magnetic energies, etc.) are compared with a converged solution at each time step and deemed to pass if the relative difference is less than $tol = 10^{-3}$ for all quantities. This verification test is relaxed for “gamma_gr” at time step 41 because the sign flips between step 40 to 42 and step 41 is two orders of magnitude smaller than the absolute value of steps 40 to 42, that is step 41 is very near the zero of “gamma_gr”. A *relative* difference test magnifies small absolute differences and is not defined at the zero of a function. The relative difference at time step 41 are well under 10^{-1} in all cases.

Solver parameters. For the 4, 8 and 16 plane case a relative residual tolerance of $rtol = 10^{-6}$, with a $V(1,1)$ -cycle, was sufficient to pass this verification test for both solvers. For the 32 plane case an $rtol = 10^{-7}$ was found to be sufficient. The 32 plane case uses a $V(5,5)$ -cycle.

4.1 Performance results

An *M3D-C1* runaway electron problem is used to evaluate a semi-coarsening multigrid solver with PBJ smoothers. This runaway electron test problem can run with four to 64 planes with 14,200 vertices per plane, resulting in 511,200 equation per plane. These test use both the CPU nodes on the Perlmutter machine, each with two 64-core AMD EPYC 7763 CPUs, and the GPU nodes with one 64-core AMD

EPYC 7763 CPU and 4 NVIDIA A100 GPUs. The CPU studies run with 32 MPI processes per node, and with 16 MPI processes per GPU node. For the CPU study, one plane is placed on each node, resulting in 4-32 node weak scaling study, and for the GPU study two nodes are used for each plane, resulting in the same number of MPI processes for each study.

Figure 2 shows the solver iteration count and solve time in each time step as reported by the $M2D - C1$ timers, with the solve time including the periodic solver setup, or refresh, for the four plane and 64 plane case. Figure 3 show the data for the scaling data for the 8, 16 and 32 plane test cases.

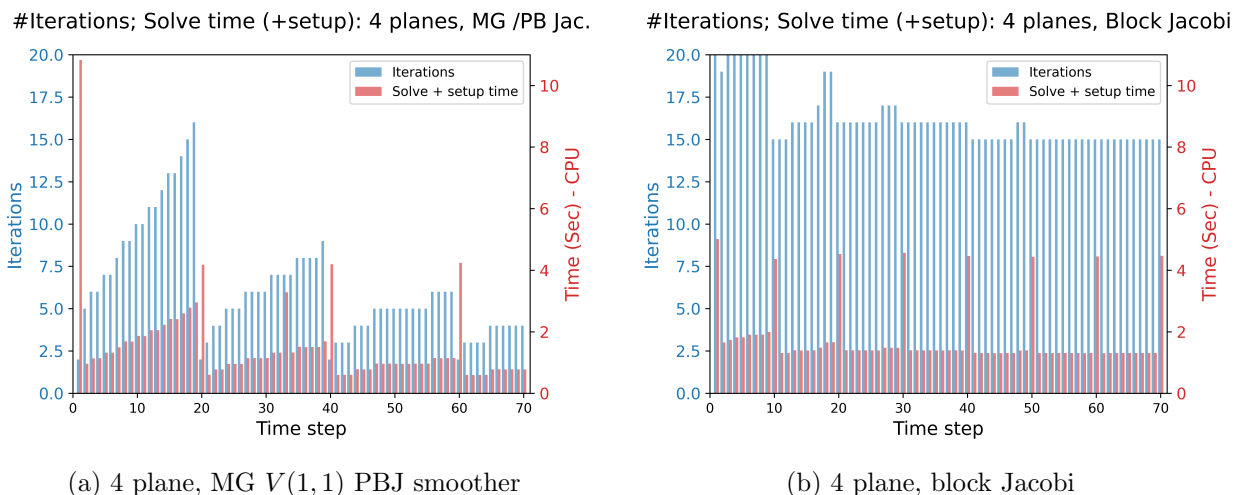
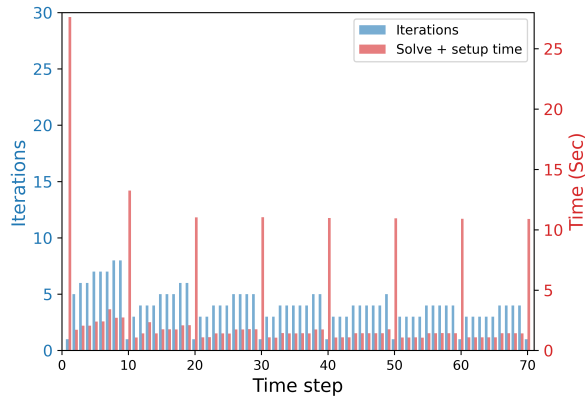


Figure 2: Iteration counts (left axis/bar) and solve times with setup (right axis/bar) vs time step, for the smallest, 4 plane test case.

This data shows that, first, the solve times are linear in the number of iterations, as expected. Second, the setup times for MG are larger than BJ and increase with problem scale (number of planes, nP). This is because both solvers factor a full plane block of the matrix, one for each plane in the BJ solver and just one for the coarse grid in the MG solver. The size of these planes relative to the number of processors is such that little speedup is observed from having nP times as many processors available in the MG case, and thus the factorization times are about the same for both solvers. The MG solver setup also includes the Galerkin coarse grid construction, which again is not significantly reduced with more compute resources per DoF on coarse grids. This cost is relatively high with only coarsening in one dimension. Since there are two coarse grids for the four plane case and six coarse grids for the 64 plane case, the cost of the coarse grid construction increases by about a factor of $3x$ in going from the four plane to the 64 plane case. Note, the solve phase and the matrix factorizations are well optimized, but there is potential for optimizing the PETSC matrix triple product setup.

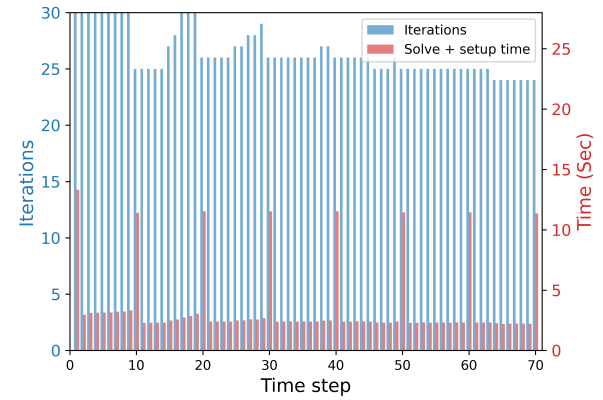
The first iteration of the MG solver with fresh coarse grid operators converges very fast. We observe a residual reduction of about nine digits in the first iteration and considerable slowing down in subsequent time steps with fresh solver. This very fast convergence is likely due to $1D$ regular grid, semi-coarsening being mathematically powerful and the mass term from the time integrator being relatively large, although this is not well understood. These test are constrained to use a minimum two iterations, which is a minimal cost and the residual reduction in the second iteration useful data. Note, there are some anomalous spikes in this data that is not understood.

#Iterations; Solve time (+setup): 8 planes, MG /PB Jac.



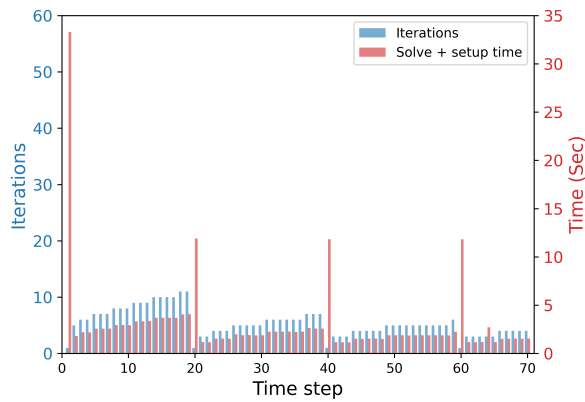
(a) 8 plane, MG $V(1,1)$ PBJ smoother

#Iterations; Solve time (+setup): 8 planes, Block Jacobi



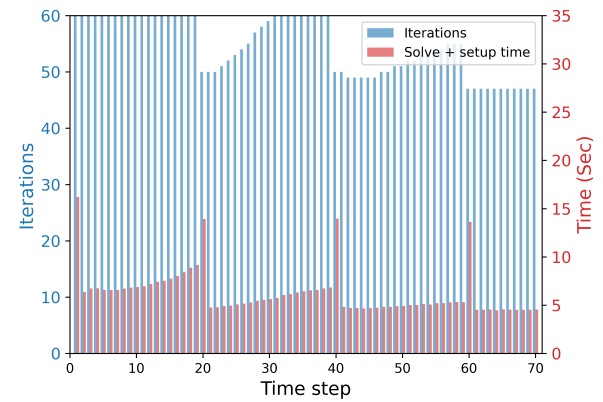
(b) 8 plane, block Jacobi

#Iterations; Solve time (+setup): 16 planes, MG /PB Jac.



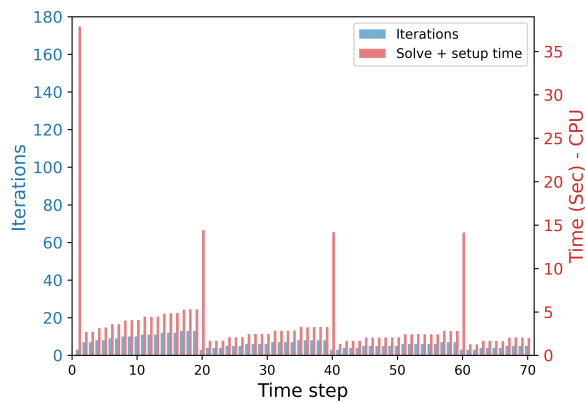
(c) 16 plane, MG $V(1,1)$ PBJ smoother

#Iterations; Solve time (+setup): 16 planes, Block Jacobi



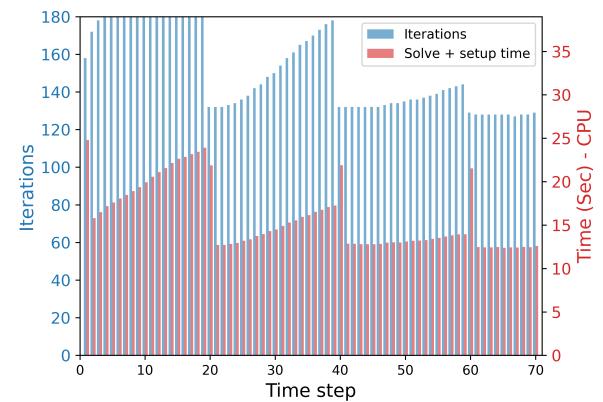
(d) 16 plane, block Jacobi

#Iterations; Solve time (+setup): 32 planes, MG /PB Jac.



(e) 32 plane, MG $V(5,5)$ PBJ smoother

#Iterations; Solve time (+setup): 32 planes, Block Jacobi



(f) 32 plane, block Jacobi

Figure 3: Iteration counts (left axis/bar), solve times with setup (right axis/bar) vs time. 8, 16 and 32 planes. Solver refresh every 20 time steps

4.1.1 Total velocity solve times

Table 1 shows the total time for the 70 time steps for the block Jacobi solver and the multigrid/point block Jacobi solver. Block Jacobi does not scale well mathematically, the number of iterations increasing, and multigrid coarse grids are relatively large with only 2:1 coarsening, resulting in growth in the setup costs.

Number of planes	4	4*	8	16	32
Multigrid / point block Jacobi	106	118	203	209	263
Block Jacobi	125	137	248	438	1,109

Table 1: Total velocity solve times (sec) as reported by the PETSC timers. *GPUs

4.1.2 Linear solver time

Table 2 shows the time for the 70 linear solves for the multigrid/point block Jacobi solver and the block Jacobi solver.

# planes	4	4*	8	16	32
MG/PBJ	90 (870)	112 (870)	156 (550)	170 (750)	217 (922)
Blk. Jac.	102 (1,145)	121 (1,322)	174 (1,895)	399 (4,209)	1,069 (11,162)

Table 2: Total linear solver, pulse solver setup, times (total number of solver iterations) as reported by the PETSC timers in seconds. *GPUs

This data shows a speedup of about $5x$ with the multigrid solver as compared to the production block Jacobi solver in *M3D-C1* on CPUs.

5 Use of devices – GPUs

A significant driver in the algorithmic designs for iterative solvers in PETSC and for the solver developed in this report is the effective use of GPUs. GPUs are very efficient in both time and energy if the application provides enough parallelism to allow many thousands of threads per GPU to work with only fast processor element (PE) synchronization, where a PE is a *streaming multiprocessor* on NVIDIA hardware and a *compute unit* on AMD hardware. The four plane test problem (Figures 2a-2b) is repeated with the use of GPUs in all numerics in Figure 4. The GPU nodes have one AMD socket on Perlmutter as opposed to two for the CPU nodes, which required the use of eight GPU nodes for a total of 32 NVIDIA A100 GPUs. Tables 1 and 2 compare the *M3D-C1* velocity solve phase and linear solver times in GPU and CPU runs.

The solve phase, the time in the Krylov iterations after the setup, are very similar, but the matrix triple product in the coarse grid constructor is $5x$ faster with (32) GPUs than with (128) CPU cores. The GPU runs use the same number of cores (MPI processes), 128, in both cases; thus, each GPU is driven by four MPI processes. Note, the solve and setup in time step 20 is less than the solve only in time step 19, indicating that this refresh period of 20 is far larger than is optimal on GPUs.

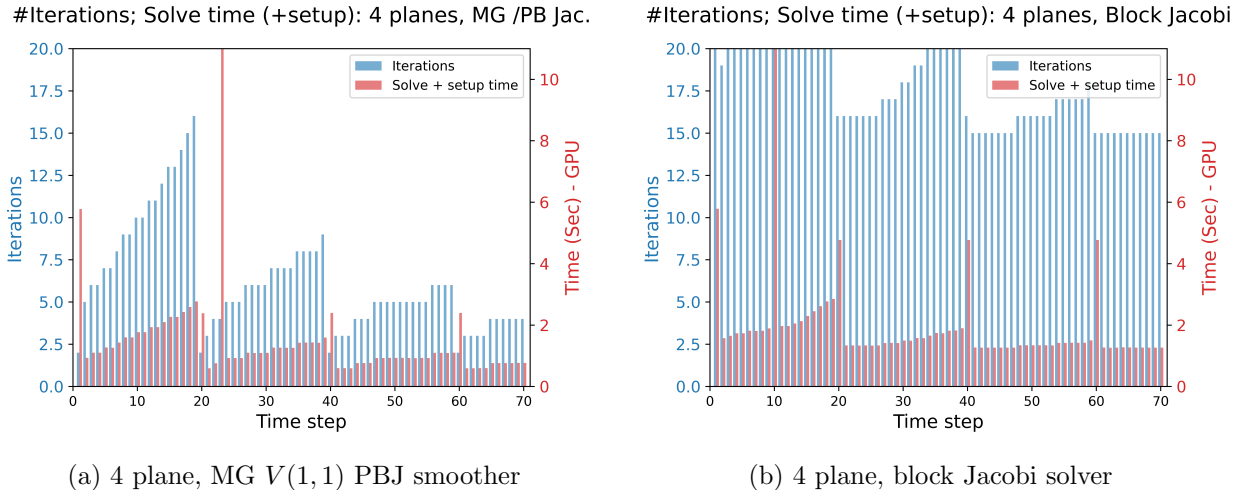


Figure 4: Four plane test case using GPUs

6 Conclusion

This report develops a toroidal semi-coarsening, geometric multigrid solver, with algebraic coarse grids for $M3D-C1$ with with point block Jacobi (PBJ) smoothers in the PETSC solver framework. The new solver sped the largest test case, 32 plane, by $5x$, and there are many optimizations left to explore: the most obvious of which is adding $2D$ multigrid to the plane to develop a full $3D$ MG solver, but improving the smoothers beyond point-wise solvers is no less important. An effective full $3D$ MG would reduce the coarse grids exponentially, relieving pressure on coarse grids that have limited amounts of parallelism. Given the large anisotropies, high-order accurate FE, mixed zeroth, first and second derivative degrees of freedom, on complicated fourth order systems, these are challenging problems and the power of (unstructured) geometric MG in the poloidal plane is a likely candidate [1, 2], and algebraic multigrid may be be feasible.

The relatively simple solver presented here is demonstrated to be effective mathematically, especially when the preconditioner is refactored, refreshed, for each solve of these nonlinear equations. However, this refresh cost is high. These costs come from the coarse grid, full plane, direct factorization and, more significantly, the Galerkin coarse grid construction. $3D$ multigrid will effectively eliminate the coarse grid factorization cost and greatly reduce the coarse grid operator construction costs.

The second primary area of improvement for MG solvers is expanding the options for the blocks in the point (small) block Jacobi smoothers. The blocks in the current PBJ smoothers can be enlarged to some extent, so as to provide more powerful smoothers, before the poor scaling of direct solvers kicks in. The appeal of PBJ smoothers is the ability to use dense linear algebra (explicit inverses and BLAS2 inverse application), which performs exceptionally well on GPUs, but increasing the block size adds sparsity to these sub-solves. Sparse batch solvers are a potential option, but they tend to be simple and do not scale well mathematically [3]. The choices for enlarging these blocks are 1) cluster on the poloidal plane, 2) grow domains in the toroidal direction from each vertex of root planes, or 3) compose these two strategies. Furthermore, the solver domains, could be overlapped, to provide very powerful smoothers. It is possible that different designs would be optimal for each of the three equations (U, ω, χ) – in a *FieldSplit* smoother – because the each of these equations represent distinct waves in the system.

Some further comments and suggestions for future work are as follows.

- Add the 64 plane test with GPUs.
- 3D MG will greatly reduce the memory footprint of both the coarse grid factorization and of the coarse grids themselves, allowing for larger process subdomains, which will increase available parallelism and thereby increase throughput, especially on GPUs.
- The choice of using Galerkin coarse grid operators is driven by expediency, but using the $M3D - C1$ operator construction to generate the coarse grids would avoid the high memory complexity of the current matrix triple products (Kokkos, cusparse, hipsparse) available in PETSC, and would provide better quality coarse grid operators.
- The linear toroidal interpolation is lower than is recommended by multigrid theory for the cubic spaces in the toroidal direction. Adding a quadratic term⁵ to the coarse grid space would be sufficient in theory and may increase the convergence rate with trivial extra cost.

The data, run and plot scripts, inputs and README-solver-paper.txt file for reproducibility data are in /global/cfs/projectdirs/mp288/jinchen/M3DC1/WORK/SPRC-m04-3D-03-TEST/ at NERSC.

Acknowledgments

This work was supported in part by the U.S. Department of Energy, Office of Science, Office of Fusion Energy Sciences and Office of Advanced Scientific Computing Research, Scientific Discovery through Advanced Computing (SciDAC) program through the FASTMath Institute under Contract No. DE-AC02-05CH11231 at Lawrence Berkeley National Laboratory. This research used resources of the National Energy Research Scientific Computing Center, a DOE Office of Science User Facility supported by the Office of Science of the U.S. Department of Energy under Contract No. DE-AC02-05CH11231 using NERSC award ASCR-ERCAP0030112.

References

- [1] M. F. Adams. *Multigrid Equation Solvers for Large Scale Nonlinear Finite Element Simulations*. Ph.D. dissertation, University of California, Berkeley, 1998. Tech. report UCB//CSD-99-1033.
- [2] Mark F. Adams and Matthew K. Knepley. A bespoke multigrid approach for magnetohydrodynamics models of magnetized plasmas in petsc, 2023.
- [3] Mark F. Adams, Peng Wang, Jacob Merson, Kevin Huck, and Matthew G. Knepley. A performance portable, fully implicit landau collision operator with batched linear solvers. *SIAM Journal on Scientific Computing*, 47(2):B360–B381, 2025.
- [4] James H. Adler, Thomas R. Benson, Eric C. Cyr, Patrick E. Farrell, Scott P. MacLachlan, and Ray S. Tuminaro. Monolithic multigrid methods for magnetohydrodynamics. *SIAM Journal on Scientific Computing*, 43(5):S70–S91, 2021.

⁵ $\frac{L}{8}$ in an off-diagonal of the current diagonal blocks for the mid-plane interpolation, $L = 2\pi R/NP$.

- [5] Kolbein Bell. A refined triangular plate bending finite element. *International Journal for Numerical Methods in Engineering*, 1(1):101–122, 1969.
- [6] L. Chacón. An optimal, parallel, fully implicit newton–krylov solver for three-dimensional viscoresistive magnetohydrodynamics. *Physics of Plasmas*, 15(5):056103, 02 2008.
- [7] S.C. Jardin. A triangular finite element with first-derivative continuity applied to fusion mhd applications. *Journal of Computational Physics*, 200(1):133–152, 2004.
- [8] U. Trottenberg, C. W. Oosterlee, and A. Schüller. *Multigrid*. Academic Press, London, 2000.

A Appendix: The Resistive MHD Equations

This appendix sketches the numerical methods in the evolution of the momentum equations with a focus on the algebraic form of the diagonal blocks of the Jacobian matrix in *M3D-C1*, which is of the most relevance to algebraic solvers.

$$\frac{\partial n}{\partial t} + \nabla \cdot (n\mathbf{v}) = 0 \quad \text{continuity} \quad (1)$$

$$\frac{\partial \mathbf{B}}{\partial t} = \nabla \times [\mathbf{v} \times \mathbf{B} - \eta \mathbf{J}] \quad \text{Maxwell} \quad (2)$$

$$nM_i \frac{d\mathbf{v}}{dt} + \nabla p - \nu \nabla^2 \mathbf{v} = \mathbf{J} \times \mathbf{B} \quad \text{momentum} \quad (3)$$

$$\mathbf{E} + \mathbf{v} \times \mathbf{B} = \eta \mathbf{J} + \frac{1}{ne} (\mathbf{J} \times \mathbf{B} - \nabla p_e - \nabla \cdot \Pi_e) \quad \text{Ohm's} \quad (4)$$

$$\frac{\partial p}{\partial t} + \mathbf{v} \cdot \nabla p + \gamma p \nabla \cdot \mathbf{v} = (\gamma - 1) [\eta \mathbf{J}^2 - \Pi : \nabla \mathbf{v}] \quad \text{energy} \quad (5)$$

η : resistivity

μ : viscosity

A.1 Dimensionless Scaling

NEWDOC-latest P41, P75, The momentum equation:

$$nM_i \frac{d\mathbf{v}}{dt} + \nabla p - \nu \nabla^2 \mathbf{v} = \mathbf{J} \times \mathbf{B} \quad (6)$$

$$n_0 \tilde{n} M_i \frac{v_0}{t_0} \frac{d\tilde{\mathbf{v}}}{d\tilde{t}} + \frac{p_0}{l_0} \tilde{\nabla} \tilde{p} - \frac{\nu_0 v_0}{l_0^2} \tilde{\nu} \tilde{\nabla}^2 \tilde{\mathbf{v}} = J_0 B_0 \tilde{\mathbf{J}} \times \tilde{\mathbf{B}} \quad (7)$$

$$\frac{l_0^2}{t_0^2} \frac{\mu_0 n_0 M_i}{B_0^2} \tilde{n} \frac{d\tilde{\mathbf{v}}}{d\tilde{t}} + \frac{\mu_0 p_0}{B_0^2} \tilde{\nabla} \tilde{p} - \frac{\nu_0 v_0 \mu_0}{B_0^2 l_0} \tilde{\nu} \tilde{\nabla}^2 \tilde{\mathbf{v}} = \tilde{\mathbf{J}} \times \tilde{\mathbf{B}} \quad (8)$$

$$\tilde{n} \frac{d\tilde{\mathbf{v}}}{d\tilde{t}} + \tilde{\nabla} \tilde{p} - \tilde{\nu} \tilde{\nabla}^2 \tilde{\mathbf{v}} = \tilde{\mathbf{J}} \times \tilde{\mathbf{B}} \quad (9)$$

where

$$t_0 = l_0 \left[\frac{\mu_0 n_0 M_i}{B_0^2} \right]^{\frac{1}{2}}, p_0 = \frac{B_0^2}{\mu_0}, J_0 = \frac{B_0}{\mu_0 l_0}, \mathbf{v}_0 = \frac{l_0}{t_0}, \nu_0 = \frac{B_0^2 t_0}{\mu_0} = \frac{n_0 M_i}{t_0} l_0^2$$

The magnetic field evolution equation (electron form) is:

$$\frac{\partial \mathbf{B}}{\partial t} = \nabla \times [\mathbf{v} \times \mathbf{B} - \eta \mathbf{J}] \quad (10)$$

$$\frac{\partial \tilde{\mathbf{B}}}{\partial \tilde{t}} = \tilde{\nabla} \times \left[\tilde{\mathbf{v}} \times \tilde{\mathbf{B}} - \frac{\eta_0 t_0}{\mu_0 l_0^2} \tilde{\eta} \tilde{\mathbf{J}} \right] \quad (11)$$

where $\eta_0 = \frac{\mu_0 l_0^2}{t_0} = B_0 l_0 \left[\frac{\mu_0}{n_0 M_i} \right]^{\frac{1}{2}}$. If \mathbf{B} is given in Tesla and all the lengths are given in meters, then $B_0 = l_0 = 1$, and the only quantity needs to be scaled is the density n_0 in units of 10^{20} .

A.2 Neumann Boundary Condition

regularize the solution by adding a small term ϵv to the equation, $\epsilon \leq 10^{-6}$. for example

$$\nabla^2 \chi - \epsilon \chi = f_\chi$$

to remove the null space in the chi part of equations. So the magnitude of χ doesn't matter, its gradient $\nabla_\perp \chi$ matters.

A.3 Parabolization

let $\dot{\mathbf{v}} \equiv \frac{\partial \mathbf{v}}{\partial t}$ we have the ideal MHD momentum equation:

$$n_0 \dot{\mathbf{v}} + \nabla p = [(\nabla \times \mathbf{B}) \times \mathbf{B}] \quad (12)$$

take its time derivative

$$n_0 \ddot{\mathbf{v}} + \nabla \dot{p} = \left[\left(\nabla \times \dot{\mathbf{B}} \right) \times \mathbf{B} + (\nabla \times \mathbf{B}) \times \dot{\mathbf{B}} \right] \quad (13)$$

Substitute the ideal MHD equation for $\dot{\mathbf{B}}$ and \dot{p}

$$\dot{\mathbf{B}} = \nabla \times [\mathbf{v} \times \mathbf{B}] \quad (14)$$

$$\dot{p} = -\mathbf{v} \cdot \nabla p - \gamma p \nabla \cdot \mathbf{v} \quad (15)$$

we get the parabolization operator

$$\mathcal{L}(\mathbf{v}) = \{ \nabla \times [\nabla \times (\mathbf{v} \times \mathbf{B})] \} \times \mathbf{B} + \{ (\nabla \times \mathbf{B}) \times \nabla \times (\mathbf{v} \times \mathbf{B}) \} + \nabla (\mathbf{v} \cdot \nabla p + \gamma p \nabla \cdot \mathbf{v}) \quad (16)$$

with the parabolization, the momentum equation becomes:

$$\{ n - \theta^2 \delta t^2 \mathcal{L} \} \frac{\partial \mathbf{v}}{\partial t} + n \mathbf{v} \cdot \nabla \mathbf{v} + \nabla p - \nu \nabla^2 \mathbf{v} = [(\nabla \times \mathbf{B}) \times \mathbf{B}] \quad (17)$$

Then we can advance the velocity as follow

$$\begin{aligned} \{ n - \theta^2 \delta t^2 \mathcal{L} \} \mathbf{v}^{n+1} + \theta \delta t (n \mathbf{v}^{n+1} \cdot \nabla \mathbf{v}^n + n \mathbf{v}^n \cdot \nabla \mathbf{v}^{n+1}) - \nu \theta \delta t \nabla^2 \mathbf{v}^{n+1} = \\ \{ n - \theta^2 \delta t^2 \mathcal{L} \} \mathbf{v}^n - (1 - 2\theta) \delta t (n \mathbf{v}^n \cdot \nabla \mathbf{v}^n) + \delta t \{ -\nabla p + [(\nabla \times \mathbf{B}) \times \mathbf{B}] \}^{n+\frac{1}{2}} \end{aligned} \quad (18)$$

A.4 Decompose the Momentum Equation in (R, ϕ, Z) coordinate system

$$\mathbf{v} = R^2 \nabla U \times \nabla \phi + R^2 \omega \nabla \phi + \frac{1}{R^2} \nabla_{\perp} \chi \quad (19)$$

The operator ∇_{\perp} denotes the gradient in the (R, Z) plane,

$$\nabla_{\perp} \chi \equiv \chi_R \hat{R} + \chi_Z \hat{Z},$$

orthogonal to $\nabla \phi$. $|\nabla \phi| = \frac{1}{R}$.

U - shear Alfvén wave, does not compress the strong toroidal magnetic field.

ω - slow wave, does not compress the toroidal magnetic field.

χ - fast wave, does compress the toroidal field.

To obtain the scalar time-advancement equations, apply 3 scalar projections:

$$\nabla \phi \cdot \nabla_{\perp} \times R^2 \quad (20)$$

$$R^2 \nabla \phi \cdot \quad (21)$$

$$\nabla_{\perp} \cdot \frac{1}{R^2} \quad (22)$$

A.5 Strong Form of \mathcal{L}

Let's set $\mathbf{Q} = \nabla \times (\mathbf{v} \times \mathbf{B})$, and rewrite the $\mathcal{L}(\mathbf{v})$ as

$$\mathcal{L}(\mathbf{v}) = (\nabla \times \mathbf{Q}) \times \mathbf{B} + \mathbf{J} \times Q + \nabla(\mathbf{v} \cdot \nabla p + \gamma p \nabla \cdot \mathbf{v})$$

The projections on (22) are applied to \mathcal{L} , for example, applying the first projection operator $\nabla \phi \cdot \nabla_{\perp} \times R^2$, we have

$$\begin{aligned} \nabla \phi \cdot \nabla_{\perp} \times R^2 \mathcal{L}(\mathbf{v}) &= \nabla \phi \cdot \nabla_{\perp} \times R^2 [(\nabla \times \mathbf{Q}) \times \mathbf{B} + \mathbf{J} \times Q + \nabla(\mathbf{v} \cdot \nabla p + \gamma p \nabla \cdot \mathbf{v})] \\ &= \nabla \phi \cdot \nabla_{\perp} \times [(\nabla \times \mathbf{Q}) \times R^2 \mathbf{B} + R^2 \mathbf{J} \times Q + R^2 \nabla(\mathbf{v} \cdot \nabla p + \gamma p \nabla \cdot \mathbf{v})] \\ &= \nabla \phi \cdot \nabla_{\perp} \times [(\nabla \times \mathbf{Q}) \times R^2 \mathbf{B}] + \nabla \phi \cdot \nabla_{\perp} \times [R^2 \mathbf{J} \times Q] \\ &\quad + \nabla \phi \cdot \nabla_{\perp} \times [R^2 \nabla(\mathbf{v} \cdot \nabla p + \gamma p \nabla \cdot \mathbf{v})] \end{aligned} \quad (23)$$

A.6 Finite Elements and Weak Form

Galerkin method: integration by parts and shifting the derivatives from the unknown to the trial function

$$\begin{aligned} \iint \nu_i [\nabla \cdot f(R, Z) \nabla \phi] dV &= - \iint f(R, Z) \nabla \nu_i \cdot \nabla \phi dV \\ \iint \nu_i [\nabla^2 f(R, Z) \nabla^2 \phi] dV &= \iint f(R, Z) \nabla^2 \nu_i \nabla^2 \phi dV \end{aligned}$$

ν_i is the i th finite element basis function.

Mass matrix and high-order stiffness matrices are of the form

$$\begin{aligned} \iint d^2 R \nu_i \nabla \phi \bullet \nabla_{\perp} \times R^2 & \rightarrow \iint d^2 R R^2 \nabla_{\perp} \nu_i \times \nabla \phi \bullet \\ \iint d^2 R \nu_i R^2 \nabla \phi \bullet & \rightarrow \iint d^2 R \nu_i R^2 \nabla \phi \bullet \\ \iint d^2 R \nu_i \nabla_{\perp} \bullet \frac{1}{R^2} & \rightarrow - \iint d^2 R \frac{1}{R^2} \nabla_{\perp} \nu_i \bullet \end{aligned} \quad (24)$$

$$U(R, Z, t^{n+1}) = \sum_{i=1}^{18} U_i^n \nu_i(R, Z)$$

These 3 projections, together with the form of the velocity field, have the effect of approximately separating the dynamics associated with each of the three MHD waves into separate diagonal blocks.

$$\begin{bmatrix} [\cdot]_U & & \\ & [\cdot]_{\omega} & \\ & & [\cdot]_{\chi} \end{bmatrix} \quad (25)$$

A.7 Decompose Operations on the Momentum Equation in R, ϕ, Z coordinate system

We are interested in the highest order terms on the diagonal blocks for designing preconditioners and after expanding and ordering the weak form we get:

$$\begin{aligned} \delta W_{11} = R^2 \nabla \nu_i \times \nabla \phi \bullet (\{ \nabla \times [\nabla \times (R^2 \nabla U^{n+1} \times \nabla \phi \times \mathbf{B})] \} \times \mathbf{B} + \{ \mathbf{J} \times [\nabla \times (R^2 \nabla U^{n+1} \times \nabla \phi \times \mathbf{B})] \}) \\ + R^2 \nabla \nu_i \times \nabla \phi \bullet (\nabla (R^2 \nabla U^{n+1} \times \nabla \phi \cdot \nabla p + \gamma p \nabla \cdot R^2 \nabla U^{n+1} \times \nabla \phi)) \end{aligned} \quad (26)$$

$$\begin{aligned} \delta W_{22} = \nu_i R^2 \nabla \phi \bullet (\{ \nabla \times [\nabla \times (R^2 \omega^{n+1} \nabla \phi \times \mathbf{B})] \} \times \mathbf{B}) \\ + \nu_i R^2 \nabla \phi \bullet (\{ \mathbf{J} \times [\nabla \times (R^2 \omega^{n+1} \nabla \phi \times \mathbf{B})] \} + \nabla (R^2 \omega^{n+1} \nabla \phi \cdot \nabla p + \gamma p \nabla \cdot R^2 \omega^{n+1} \nabla \phi)) \end{aligned} \quad (27)$$

$$\begin{aligned} \delta W_{33} = \frac{1}{R^2} \nabla \nu_i \bullet (\{ \nabla \times [\nabla \times (\frac{1}{R^2} \nabla_{\perp} \chi^{n+1} \times \mathbf{B})] \} \times \mathbf{B}) \\ + \frac{1}{R^2} \nabla \nu_i \bullet (\{ \mathbf{J} \times [\nabla \times (\frac{1}{R^2} \nabla_{\perp} \chi^{n+1} \times \mathbf{B})] \} + \nabla (\frac{1}{R^2} \nabla_{\perp} \chi^{n+1} \cdot \nabla p + \gamma p \nabla \cdot \frac{1}{R^2} \nabla_{\perp} \chi^{n+1})) \end{aligned} \quad (28)$$

A.8 Time Advance: split implicit method

The multiple timescales require using an implicit numerical algorithm so that the time step can be large compared to the Courant condition for the fastest wave and still maintain numerical stability. The implicit solution requires evaluating the spatial derivatives at the new time level. If we discretize the equations in

space and linearize them about the present time level, the time advance equations to go from time step n to time step $n + 1$ take the form

$$A \cdot X^{n+1} = R(X^n) \quad (29)$$

Here X^{n+1} is the complete solution $(n, \mathbf{v}, \mathbf{B}, p)$ at the new time level, the right side is a function only of the old time level and the matrix A is a very large (typically $10^7 \times 10^7$ or larger), non-diagonally dominant, non-symmetric, ill-conditioned sparse matrix. The ill-conditioning is a direct result of the fact that this matrix contains all of the MHD wave phenomena in it.

Let $t = n\delta t, x = j\delta x, s = c\frac{\delta t}{\delta x}$, then we have 3 major linear matrix solves per time-step performed sequentially

1. the velocity solve ... \mathbf{v}^{n+1}
2. the magnetic field solve ... \mathbf{B}^{n+1}
3. the pressure solve ... p^{n+1}

where \mathbf{v}^{n+1} is solved as

$$\begin{aligned} nR^2(\nu_i, \dot{U}) - n[\nu_i, \dot{\chi}] &= \dots \\ nR^2\nu_i\dot{\omega} &= \dots \\ \frac{n}{R^4}(\nu_i, \dot{\chi}) + n[\nu_i, \dot{U}] &= \dots \end{aligned} \quad (30)$$

The inner product is defined as

$$(a, b) \equiv \nabla_{\perp} a \cdot \nabla_{\perp} b = a_R b_R + a_Z b_Z$$

and the Poisson bracket as

$$[a, b] \equiv [\nabla a \times \nabla b \cdot \nabla \phi] = R^{-1}(a_Z b_R - a_R b_Z)$$

After parabolization:

$$\begin{aligned} nR^2(\nu_i, \dot{U}) - n[\nu_i, \dot{\chi}] & -\theta^2\delta t^2\{\delta W_{11}^0(\nu_i, \dot{U}) + \delta W_{11}^1(\nu_i, \dot{U}') + \delta W_{11}^2(\nu_i, \dot{U}'') + \\ & \delta W_{12}^1(\nu_i, \dot{\omega}') + \delta W_{12}^2(\nu_i, \dot{\omega}'') + \\ & \delta W_{13}^0(\nu_i, \dot{\chi}) + \delta W_{13}^1(\nu_i, \dot{\chi}') + \delta W_{13}^2(\nu_i, \dot{\chi}'')\} = \dots \\ nR^2\nu_i\dot{\omega} & -\theta^2\delta t^2\{\delta W_{21}^1(\nu_i, \dot{U}') + \delta W_{21}^2(\nu_i, \dot{U}'') + \\ & \delta W_{22}^0(\nu_i, \dot{\omega}) + \delta W_{22}^1(\nu_i, \dot{\omega}') + \delta W_{22}^2(\nu_i, \dot{\omega}'') + \\ & \delta W_{23}^0(\nu_i, \dot{\chi}) + \delta W_{23}^1(\nu_i, \dot{\chi}') + \delta W_{23}^2(\nu_i, \dot{\chi}'')\} = \dots \\ \frac{n}{R^4}(\nu_i, \dot{\chi}) + n[\nu_i, \dot{U}] & -\theta^2\delta t^2\{\delta W_{31}^0(\nu_i, \dot{U}) + \delta W_{31}^1(\nu_i, \dot{U}') + \delta W_{31}^2(\nu_i, \dot{U}'') + \\ & \delta W_{32}^0(\nu_i, \dot{\omega}) + \delta W_{32}^1(\nu_i, \dot{\omega}') + \delta W_{32}^2(\nu_i, \dot{\omega}'') + \\ & \delta W_{33}^0(\nu_i, \dot{\chi}) + \delta W_{33}^1(\nu_i, \dot{\chi}') + \delta W_{33}^2(\nu_i, \dot{\chi}'')\} = \dots \end{aligned} \quad (31)$$

B Appendix: Block Norms

The FieldSplit solvers use a (3) block Gauss-Seidel or Jacobi preconditioned GMRES solver. The efficacy of these preconditioners is a function of how strong the diagonal blocks, the actual solves in the iteration, are relative to the off-diagonal blocks. This section reports the norms of these blocks, a 3×3 scalar matrix, and the degree of diagonal dominance is indicative of the convergence rates that one can expect. The relative off-diagonal block norms is ranges between 10^{-2} to 10^{-3} , which indicates that FieldSplit should be an effective solver/smoothen.

Note: these block norm tests are in the context of plane solvers. We first extracted a single plane block from a full 3D matrix, on which the analysis was done.

To get a sense of the strength of coupling between fields, we consider symmetric diagonal scaling of the Frobenius norms of each field block. Specifically, we examine the following 3×3 coupling matrix for three test cases.

$$\begin{pmatrix} 1 & \frac{\|A_{U,\omega}\|_F}{\sqrt{\|A_{U,U}\|_F\|A_{\omega,\omega}\|_F}} & \frac{\|A_{U,\chi}\|_F}{\sqrt{\|A_{U,U}\|_F\|A_{\chi,\chi}\|_F}} \\ \frac{\|A_{\omega,U}\|_F}{\sqrt{\|A_{U,U}\|_F\|A_{\omega,\omega}\|_F}} & 1 & \frac{\|A_{\omega,\chi}\|_F}{\sqrt{\|A_{\omega,\omega}\|_F\|A_{\chi,\chi}\|_F}} \\ \frac{\|A_{\chi,U}\|_F}{\sqrt{\|A_{U,U}\|_F\|A_{\chi,\chi}\|_F}} & \frac{\|A_{\chi,\omega}\|_F}{\sqrt{\|A_{\omega,\omega}\|_F\|A_{\chi,\chi}\|_F}} & 1 \end{pmatrix}$$

The number of equations and number of non-zeros for the three test cases are given in Table 3.

	Case 1	Case 2	Case 3
Test case name	p-cpu-16F-R01	nstx_120446	numvar.NV3.mgfs
N	189 180	365 796	401 292
NNZ	46 472 313	89 557 184	98 771 994

Table 3: Number of equations and non-zeros in each test case

The coupling matrices for each case are:

$$\text{Case 1: } \begin{pmatrix} 1.0 & 1.5 \times 10^{-4} & 1.3 \times 10^{-3} \\ 1.5 \times 10^{-4} & 1.0 & 8.5 \times 10^{-4} \\ 1.3 \times 10^{-3} & 8.5 \times 10^{-4} & 1.0 \end{pmatrix}$$

$$\text{Case 2: } \begin{pmatrix} 1.0 & 2.3 \times 10^{-4} & 8.4 \times 10^{-3} \\ 2.3 \times 10^{-4} & 1.0 & 1.3 \times 10^{-3} \\ 8.4 \times 10^{-3} & 1.3 \times 10^{-3} & 1.0 \end{pmatrix}$$

$$\text{Case 3: } \begin{pmatrix} 1.0 & 5.1 \times 10^{-5} & 6.3 \times 10^{-3} \\ 5.1 \times 10^{-5} & 1.0 & 1.6 \times 10^{-2} \\ 6.3 \times 10^{-3} & 1.6 \times 10^{-2} & 1.0 \end{pmatrix}$$